Available online at www.sciencedirect.com
SCIENCE DIRECT
Journal of Power Sources 153 (2006) 319–327
JOURNAL OF POWER SOURCES
www.elsevier.com/locate/jpowsour

Solution route synthesis of InSb, Cu_6Sn_5 and Cu_2Sb electrodes for lithium batteries

T. Sarakonsri [b,1], C.S. Johnson [a,*], S.A. Hackney [b], M.M. Thackeray [a]

[a] *Electrochemical Technology and Basic Sciences Program, Chemical Engineering Division, Argonne National Laboratory, Argonne, IL 60439, USA*
[b] *Department of Metallurgical and Materials Engineering, Michigan Technological University, Houghton, MI 49931, USA*

Available online 11 July 2005

Abstract

A solution method was used to prepare InSb, Cu_6Sn_5 and Cu_2Sb intermetallic compounds that are of interest as negative electrode materials for lithium batteries. The compounds were synthesized by the reduction of dissolved transition metal- and metalloid salts with fine Zn powder. Heterogeneous redox reactions at the surface of the Zn particles resulted in fern-like dendritic structures with high surface areas. Powder X-ray diffraction and lattice imaging by transmission electron microscopy showed that the intermetallic products were highly crystalline with preferred crystallographic orientations. Mild heat-treatment of the products under argon improved their phase purity. Electrodes prepared by this method exhibited a large irreversible capacity loss on the first charge/discharge cycle. Cu_2Sb electrodes showed the greatest cycling stability; after the initial cycle, they delivered more than 230 mAh g^{-1} when cycled between 1.2 and 0.0 V versus metallic lithium, consistent with previously reported data for ball-milled Cu_2Sb electrodes.

Keywords: Lithium; Battery; Intermetallic; InSb; Cu_6Sn_5; Cu_2Sb

1. Introduction

Over the past 10 years, there has been a renewed interest in metal alloys and intermetallic compounds for replacing graphitic carbon as the anode of choice in lithium-ion batteries. The lithiation voltage of these materials is sufficiently positive of metallic lithium to minimize lithium plating (overcharge) problems. Furthermore, these materials offer a higher volumetric capacity than graphite. For example, the theoretical volumetric capacity of InSb is 1938 mAh cm^{-3} (assuming a constant electrode density of 5.7 g cm^{-3} throughout charge and discharge) compared with a theoretical 818 mAh cm^{-3} for graphite ($\rho = 2.2$ g cm^{-3}).

Intermetallic compounds can react with lithium in two distinct ways. For a binary system, the reaction can occur either by (1) lithium insertion with little or no extrusion of metal atoms from the host structure, or (2) lithium insertion into, and metal displacement from, the structure. Examples of the first case are Cu_6Sn_5 and MnSb that, on lithiation, form Li_2CuSn [1] and LiMnSb [2], respectively. In the second case, the intermetallic compound can be comprised entirely of elements that react with lithium, such as in SnSb [3], InSb [4] or Ag_3Sb [5] when discrete Li_xSn, Li_xSb, Li_xIn and Li_xAg phases are formed; alternatively, the intermetallic compound can consist of elements, only one of which reacts with lithium, as in $FeSn_2$ [6], Cu_2Sb [7] and $CoSb_3$ [8] in which case the Li_xSn or Li_xSb phases are cycled within electrochemically inactive Fe, Cu or Co metal matrices, respectively.

Electrochemical reactions of lithium with metals such as Al, Si, Sn, Sb, In, and Ag, or with the intermetallic compounds described above are typically accompanied by large increases in volume [9]. The repeated expansion and contraction that occurs during electrochemical cycling pulverizes the electrode particles. In attempts to overcome this problem, nanocomposite intermetallic electrodes have been fabricated, for example, by high-energy ball milling [6,10–11] in order to

* Corresponding author. Tel.: +1 630 252 4787; fax: +1 630 252 4176.
E-mail address: johnsoncs@cmt.anl.gov (C.S. Johnson).
[1] Present address: Department of Chemistry, Chiang Mai University, Chiang Mai 50200, Thailand.

0378-7753/$ – see front matter © 2005 Elsevier B.V. All rights reserved.
doi:10.1016/j.jpowsour.2005.05.061

control lithium diffusion lengths within the metal matrix and to minimize the loss of particle-to-particle contact during the electrochemical pulverization process.

As an alternative technique to ball milling, we have explored a solution route method to synthesize ultra-small metal and intermetallic particles at room temperature. In this paper, we report on the synthesis of InSb, Cu_6Sn_5 and Cu_2Sb powders using zinc powder to reduce metal chlorides dissolved in de-aerated, ethylene glycol [12]. Our approach is similar to that which has recently been used for producing Sn/SnSb electrode materials [13,14]. The morphological features of the materials and their electrochemical properties in lithium cells are described.

2. Experimental

2.1. Synthesis

InSb, Cu_6Sn_5 and Cu_2Sb intermetallic compounds were prepared according to the following general procedure using the chemicals listed in Table 1. Stoichiometric quantities of the metal chloride salts were dissolved in de-aerated ethylene glycol at room temperature. Thereafter, zinc powder was gradually added to the solutions with continuous stirring for 1 day. The products were filtered, washed with methanol and dried in air at 110 °C. The resulting powders were finally annealed for 20 h at either 220 or 400 °C under an argon atmosphere. The reactions for the preparation of InSb, Cu_6Sn_5 and Cu_2Sb are:

$$InCl_3 + SbCl_3 + 3Zn \rightarrow InSb + 3ZnCl_2 \quad (1)$$

$$6CuCl_2 + 5SnCl_2{\cdot}2H_2O + 11Zn \rightarrow Cu_6Sn_5 + 11ZnCl_2 + 10H_2O \quad (2)$$

$$4CuCl_2 + 2SbCl_3 + 7Zn \rightarrow 2Cu_2Sb + 7ZnCl_2 \quad (3)$$

The $ZnCl_2$ by-product, which is soluble in the ethylene glycol solvent, was removed during multiple filtering and washing steps. A small excess of Sn (2 at.%) was used for the preparation of Cu_6Sn_5 because Cu_3Sn had a tendency to form during the reactions.

InSb electrode powders were also prepared by high-energy ball milling according to a method described elsewhere [15] in order to compare the electrochemical performance of these electrodes with those synthesized by the solution route method.

Table 1
Reagents used for the preparation of intermetallic compounds

Reagent	Vendor	Purity (%)
$CuCl_2$	Fisher Scientific	99.98
$SbCl_3$	Alfa Aesar	99.0
$SnCl_2{\cdot}2H_2O$	Aldrich	99.0
$InCl_3$	Alfa Aesar	99.99
Zn powder	Fisher Scientific	99.95
Ethylene glycol	Fisher Scientific	99

2.2. Structural and physical characterization

Powder X-ray diffraction patterns of InSb, Cu_6Sn_5 and Cu_2Sb products prepared by the solution route were recorded before and after thermal annealing under argon. Data were collected on a Siemens D-5000 diffractometer with Cu Kα radiation between 10° and 80° 2θ at a scan rate of 0.6° $2\theta\,min^{-1}$. Impurities in the reaction products were identified with the aid of the JCPDS database [16].

High-resolution images of the intermetallic products were collected on a JEOL-JEM 4000FX-1 transmission electron microscope (TEM) under an accelerating voltage of 200 keV. Samples were prepared for the electron microscope by a standard procedure described elsewhere [17]. Convergent beam electron diffraction (CBED) and lattice imaging methods were used to analyze the samples.

A computer-controlled simultaneous TG/DTA EXSTAR 6300 unit (Seiko Instruments Inc.) was used for thermogravimetric analyses of the samples in flowing argon.

2.3. Electrochemical measurements

Lithium cells were constructed according to the following procedure. The intermetallic electrode consisted of 84% (by mass) of the active compound (InSb, Cu_6Sn_5 or Cu_2Sb) intimately mixed with 8% polyvinylidene difluoride (PVDF) polymer binder (Kynar, Elf-Atochem), 4% acetylene black (Cabot) and 4% graphite (SFG-6, Timcal). Electrode laminates were cast from slurries of the electrode powders in 1-methyl-2-pyrrolidinone (NMP, Aldrich) onto Cu current collector foils using a doctor blade. The laminates were subsequently dried, first at 75 °C for 10 h and, thereafter, under vacuum at 70 °C for 12 h. The electrolyte was 1 M $LiPF_6$ in ethylene carbonate (EC):di-ethyl carbonate (DEC) (1:1 weight mixture; Merck). Electrodes were evaluated at room temperature in coin-type cells (size CR2032, Hohsen) with a lithium-foil counter electrode (FMC Corporation) and a polypropylene separator (Celgard 2400). Cells were assembled inside a He-filled glove box (<5 ppm H_2O and O_2) and cycled on a Maccor Series 2000 tester under galvanostatic mode with a constant current density of 0.1–0.2 mA cm^{-2} in the voltage window of 1.5–0.5 V for InSb, 1.5–0.1 V for Cu_6Sn_5 and 1.2–0 V for Cu_2Sb.

3. Results and discussion

3.1. The synthetic process

Intermetallic compounds such as InSb, Cu_6Sn_5, and Cu_2Sb are typically synthesized by high-energy ball milling and/or firing of elemental powders [1,7,15]. This procedure

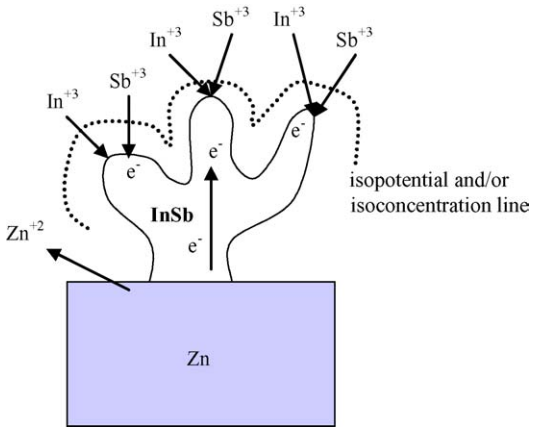

Fig. 1. Schematic illustration of the mechanism of dendrite nucleation from reaction of $InCl_3$ and $SbCl_3$ with Zn metal.

necessitates repetitive grinding, sieving and size reduction of the particles; it can lead to impurities in the sample such as metal oxides at the particle surface [18]. By contrast, the solution route process described in this paper to prepare InSb, Cu_6Sn_5 and Cu_2Sb powders is based on a heterogeneous redox reaction [12,19]. The redox reaction occurs at the surface of the solid Zn metal particles and results in nanoscopic structures with high surface areas, the morphology of which can be tailored or modified by further thermal treatment [12]. The electroless redox reaction occurs at a point of contact on the Zn metal surface with the dissolved metal ions, resulting in the growth of intermetallic crystals with dendritic features. The electrochemical overpotential at the solution/precipitate interface produces an electric field that focuses the ionic current to the dendrite tip. This effect is depicted schematically in Fig. 1. This concept has been considered previously as a rationalization for dendrite formation during electroplating [20] and it is applied here as the hypothesis to the formation mechanism of these dendritic intermetallic materials. Because the redox reaction is limited by mass-transport, the solution route method is conducive to the homogenous substitution of elements within the intermetallic structures. For example, the Ni- and Fe-substituted compounds, Cu_5NiSn_5 and Cu_5FeSn_5, can be synthesized by this process [21].

3.2. XRD analysis

The X-ray diffraction patterns of the reaction products before and after annealing the InSb, Cu_6Sn_5, and Cu_2Sb samples under argon are shown in Figs. 2–4, respectively. The X-ray pattern shows that the yield of InSb prior to annealing is much lower than expected; the product contained a substantial amount of unreacted In and Sb (Fig. 2a). After annealing, the predominant product was InSb, which is indexed according to its face-centered-cubic (fcc) symmetry (space group *F*4-3*m*) in Fig. 2b. However, some of the unreacted indium in the un-annealed sample was oxidized to In_2O_3 during thermal treatment; as a consequence of this reaction, the annealed product contained a small amount of residual, unreacted Sb.

For the Cu_6Sn_5 sample, the reaction product before the annealing step showed a relatively small amount of Cu_6Sn_5 and a large amount of unreacted tin (Fig. 3a); surprisingly, the unreacted copper in its expected fcc form was not evident in the X-ray diffraction pattern. Fig. 3b shows that after the annealing step, the product consisted predominantly of Cu_6Sn_5 and Cu_3Sn, indicating that the unreacted copper in the un-annealed sample must have been present as an amorphous component. We will return to this anomaly later in the paper.

In contrast to InSb and Cu_6Sn_5, the solution route method provided a high yield of Cu_2Sb; this phase dominated the X-ray diffraction pattern (Fig. 4a). A minor amount of Sb_2O_3 was also detected in the un-annealed sample; this impurity phase remained in the sample after thermal treatment. A decrease in the full-width at half maximum of the peaks in

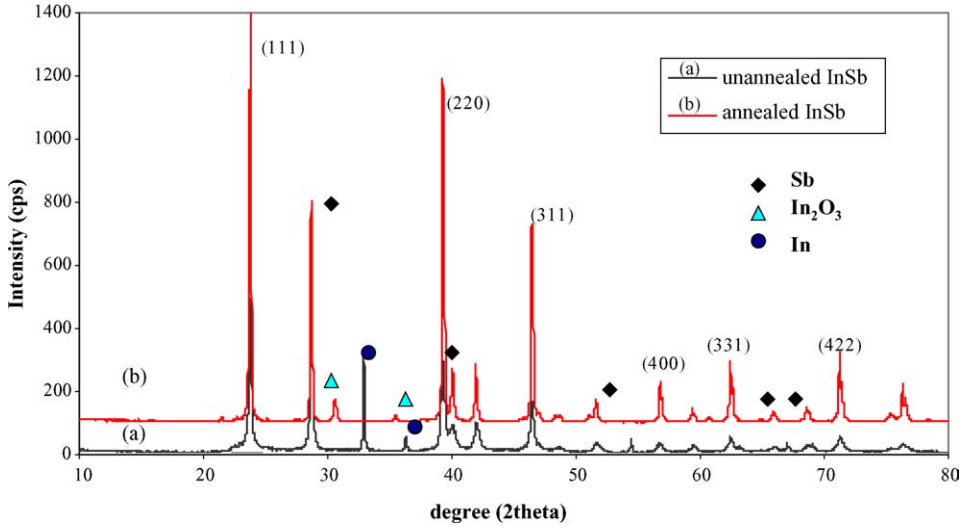

Fig. 2. X-ray diffraction patterns of (a) as-prepared (un-annealed) InSb and (b) annealed InSb synthesized from non-aqueous Zn reduction reaction.

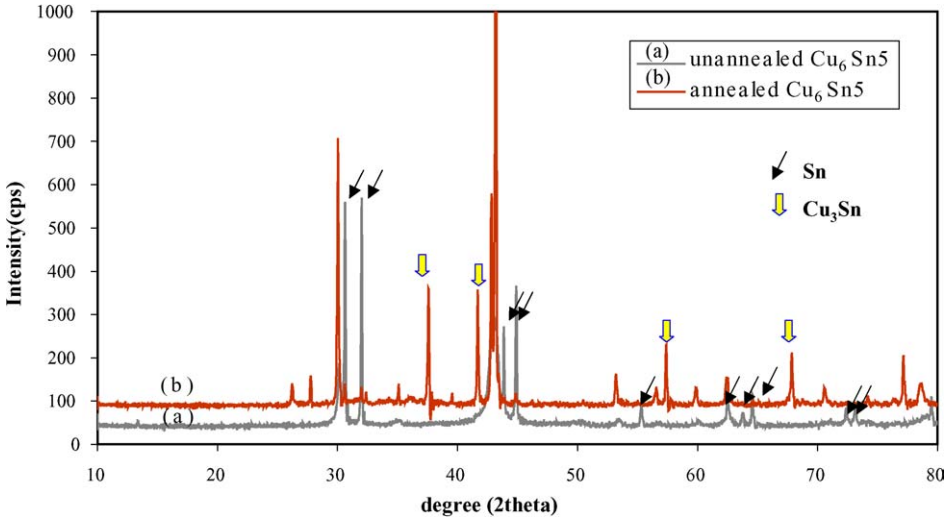

Fig. 3. X-ray diffraction patterns of (a) as-prepared (un-annealed) Cu_6Sn_5 and (b) annealed Cu_6Sn_5 synthesized from non-aqueous Zn reduction reaction.

Figs. 2–4 indicated that, in general, the crystallinity of the InSb, Cu_6Sn_5, and Cu_2Sb components was increased by the annealing step.

3.3. TEM analysis

The morphology of as-precipitated and annealed InSb, Cu_6Sn_5, and Cu_2Sb powders is shown by TEM in Figs. 5–7. The particle shape is reminiscent of the dendrite morphology often observed in solidification processing of materials; we propose they propagate and develop through the mechanism of 'diffusional instability' [22], although in the case of a heterogeneous electron-transfer process such as illustrated in Fig. 1, the small curvature of the electric field at the solid–liquid interface may also contribute to the instabilities and roughness elements responsible for tip propagation and dendrite formation [20]. An alternative explanation for the observed morphology is that the dendrites form by the agglomeration of random particle nuclei. However, a comparison of convergent beam electron diffraction patterns from various points on a dendrite and selected area electron diffraction patterns of the entire dendrite particles has revealed strong crystalline texture with different regions of the dendrite having similar crystallographic orientations [12]. Such an observation is also consistent with the diffusional instability growth mechanism of the particle dendrites as opposed to random agglomeration of particle nuclei, which would be expected to show a random polycrystalline structure.

A combination of energy dispersive X-ray spectroscopy and electron diffraction has also revealed that some impurity phases, such as metallic Sb in the as-precipitated InSb stoichiometry and the amorphous Cu-rich Sn-phase in the as-precipitated Cu_6Sn_5 stoichiometry, form as isolated particles during synthesis. These impurities form separate dendrites

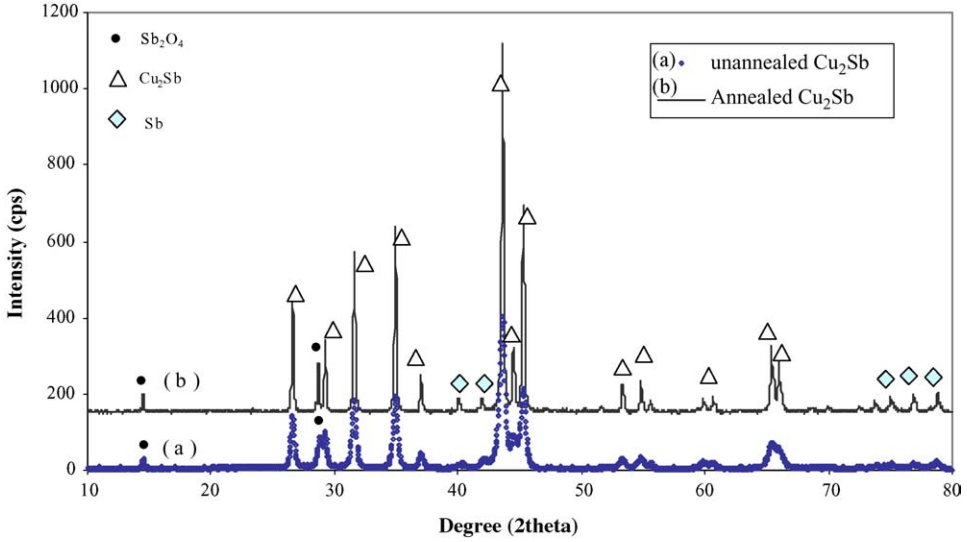

Fig. 4. X-ray diffraction patterns of (a) as-prepared (un-annealed) Cu_2Sb and (b) annealed Cu_2Sb synthesized from non-aqueous Zn reduction reaction.

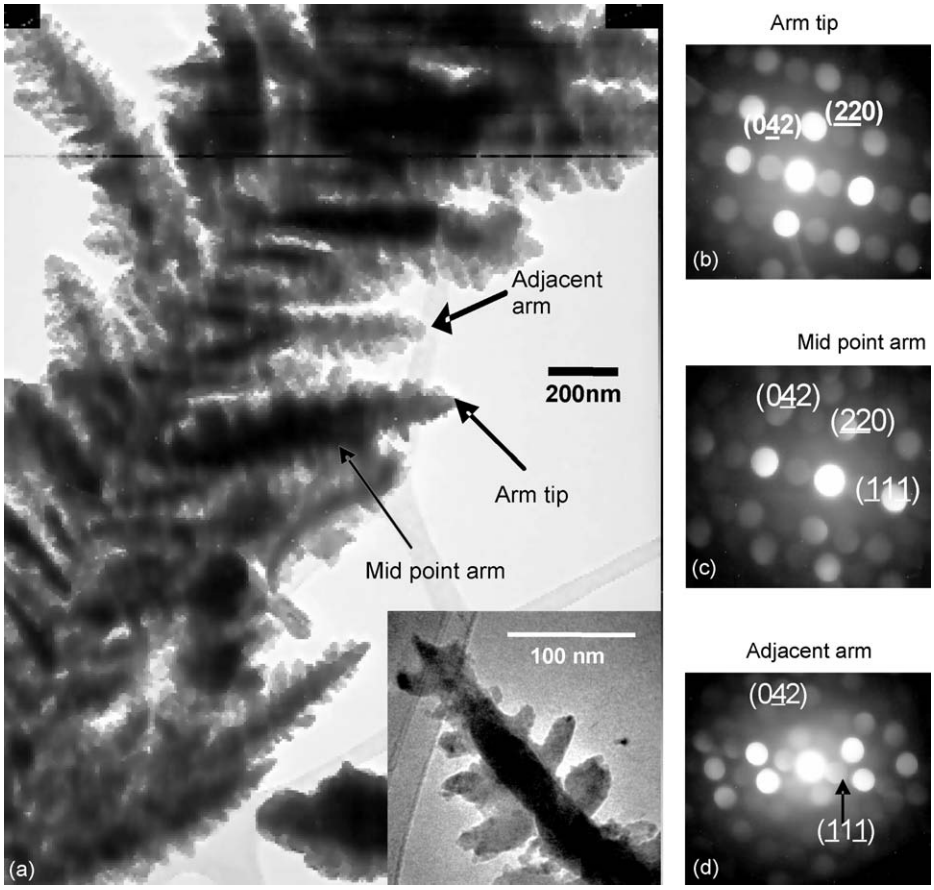

Fig. 5. (a) As-precipitated (un-annealed) InSb morphology and annealed microstructure (inset). (b–d) CBED patterns from various points on the dendrite particle indicated by arrows.

from the InSb, and Cu_6Sn_5 compound crystals. As an example, Fig. 8 shows an isolated amorphous Cu rich particle from the Cu_6Sn_5 synthesis. These TEM data emphasize that control of the chemistry and kinetics of the precipitation process is critical for engineering a target particle size and composition when this route for preparing intermetallic compounds is used.

3.3.1. InSb

The morphology of an un-annealed InSb sample is shown in Fig. 5. Analysis by electron diffraction and energy dispersive spectrometry (EDS) indicates that the dendrites were comprised of crystalline InSb, crystalline Sb and a material that was unstable in the electron beam. Equiaxed In particles were also observed in this specimen. The convergent beam electron diffraction (CBED) shows the growth of the InSb primary dendrite arms occurs in a direction perpendicular to the close packed $(2\,\underline{2}\,0)$ planes (Fig. 5b–d). By careful CBED analysis, it was observed that some misorientation exists between adjacent secondary dendrite arms (Fig. 5a). The $[1\,\underline{1}\,\underline{2}]$ zone axis showing $(\underline{1}\,1\,\underline{1})$, $(0\,\underline{4}\,2)$ and $(2\,\underline{2}\,0)$ reflections was observed in the arm tip (Fig. 5b) and at the mid-point of the arm (Fig. 5c). The disappearance of the $(2\,\underline{2}\,0)$ reflection in the $[1\,\underline{1}\,\underline{2}]$ zone axis is an indication of the misorientation that occurs in the adjacent secondary dendrite (Fig. 5d). In fact, however, the electron diffraction indicated the InSb dendrites have only a slight misorientation between crystalline domains, the maximum misorientation about [0 0 1] was observed to be typically 15.5°.

3.3.2. Cu_6Sn_5

The dendritic morphology of an un-annealed Cu_6Sn_5 sample is shown in Fig. 6a; the electron diffraction (SAD) patterns showed that the dendrites consisted of Cu_6Sn_5 and Cu_3Sn phases (Fig. 6b). Another unidentified constituent of the dendrites was unstable under the electron beam. On thermal treatment, the morphology changed from dendritic to an amorphous spherical shape, as shown in Fig. 6c. EDS analyses provided evidence of some Zn in the Cu_6Sn_5 structure indicating that some residual, unreacted zinc from the initial reaction was present in the samples. EDS analyses of the amorphous component of the dendrite showed that this component contained significantly more copper (Cu $K\alpha_1$/Sn $K\alpha_1$ peak area ratio = 5.055) than a Cu_6Sn_5 component in which the Cu $K\alpha_1$/Sn $K\alpha_1$ peak area ratio was 2.436. Cu_3Sn was identified by XRD in the annealed sample (Fig. 3).

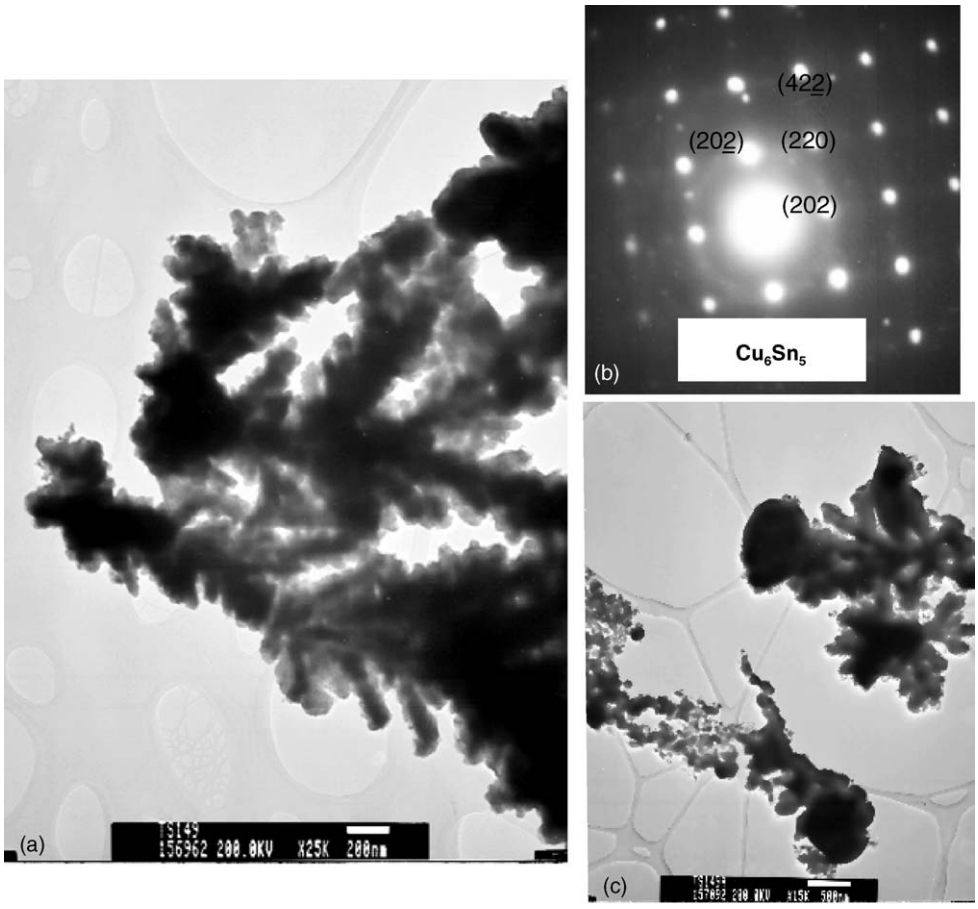

Fig. 6. (a) As-precipitated (un-annealed) Cu_6Sn_5 morphology, (b) Cu_6Sn_5 single particle SAD pattern, and (c) annealed Cu_6Sn_5.

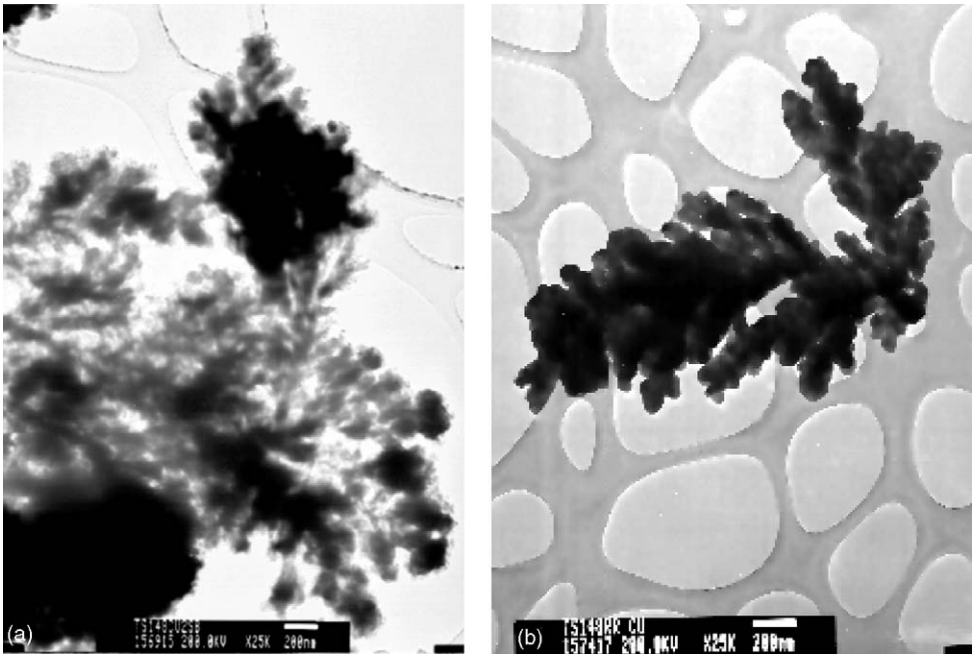

Fig. 7. (a) As-precipitated (un-annealed) Cu_2Sb morphology and (b) annealed Cu_2Sb.

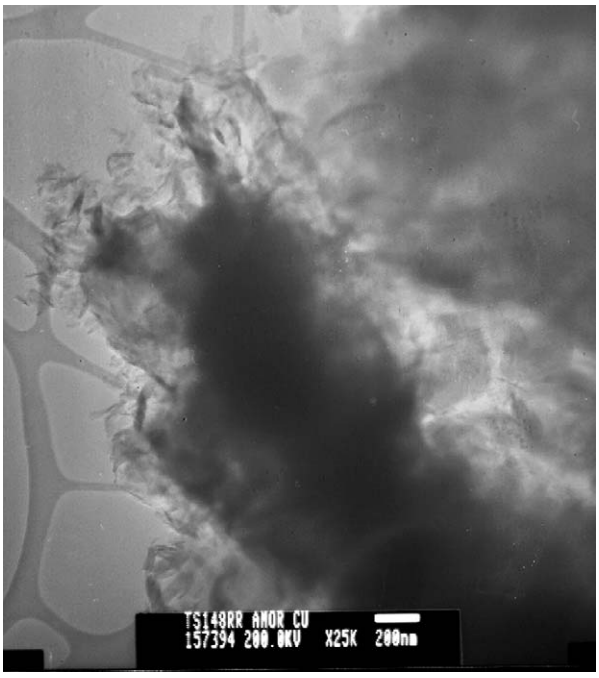

Fig. 8. TEM image of an amorphous, Cu-rich particle in the Cu_6Sn_5 as-preticipated (un-annealed) sample.

3.3.3. Cu_2Sb

The dendritic morphology of a precipitated Cu_2Sb sample prior to annealing is shown in Fig. 7a; the corresponding SAD pattern (not shown) revealed that the dendrite was comprised of crystalline Cu_2Sb and Sb phases, the relative amounts of which varied from dendrite to dendrite. Some dendrites were Sb-rich (the Cu $K\alpha_1$/Sb $K\alpha_1$ peak area ratios were between 3.21 and 1.52), while others were Cu-rich (the Cu $K\alpha_1$/Sb $K\alpha_1$ 3.21–1.52). Regions of pure Cu were also detected in the sample. The TEM images of the Cu-rich regions were amorphous, as in the Cu_6Sn_5 samples (Fig. 8). It was also observed by TEM that certain regions of the powder were unstable to the electron beam. These regions either melted or decomposed, forming particles of circular cross section when exposed to the beam. EDS analyses of these regions showed a high copper content (Cu $K\alpha_1$/Sb $K\alpha_1$ peak area ratio = 39.8), compared to a typical TEM-stable region of the dendrite (Cu $K\alpha_1$/Sb $K\alpha_1$ = 1.74).

Table 2
Weight lost during the annealing of Cu_2Sb, Cu_6Sn_5 and InSb products

	Weight lost (%)
InSb	3.49 ± 0.08
Cu_6Sn_5	8.49 ± 1.21
Cu_2Sb	6.53 ± 3.17

With extended observation under the electron beam, unstable particles decomposed into smaller particles that adhered to the surrounding carbon support web. The SAD patterns of these small particles revealed rhombohedral Sb (*R*-3*m*), cubic Sb_2O_4 (*Fd*-3*m*), and fcc Cu.

The microstructure of the annealed Cu_2Sb sample observed under TEM is shown in Fig. 7b. The dendrite morphology was still apparent in certain regions after the annealing process; an equiaxed morphology was also present.

The X-ray diffraction patterns in Figs. 2–4 clearly show that annealing the powders increased the yield of the intermetallic phases; particularly high yields were obtained for the copper-based compounds, Cu_6Sn_5 and Cu_2Sb. The absence of any unreacted copper metal in un-annealed Cu_6Sn_5 and Cu_2Sb samples leaves the presence of an amorphous copper-

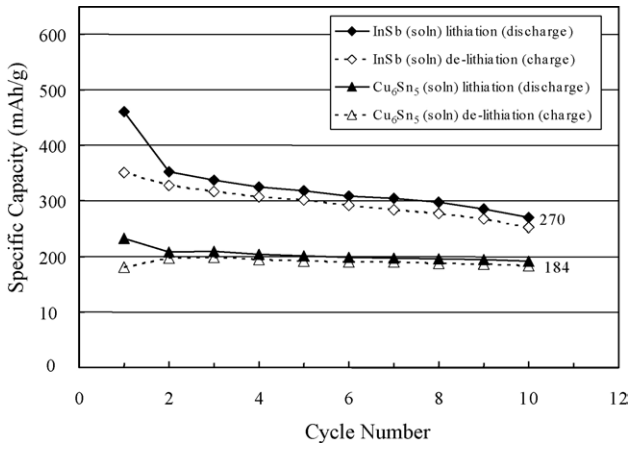

Fig. 10. Capacity plots of InSb and Cu_6Sn_5 electrodes.

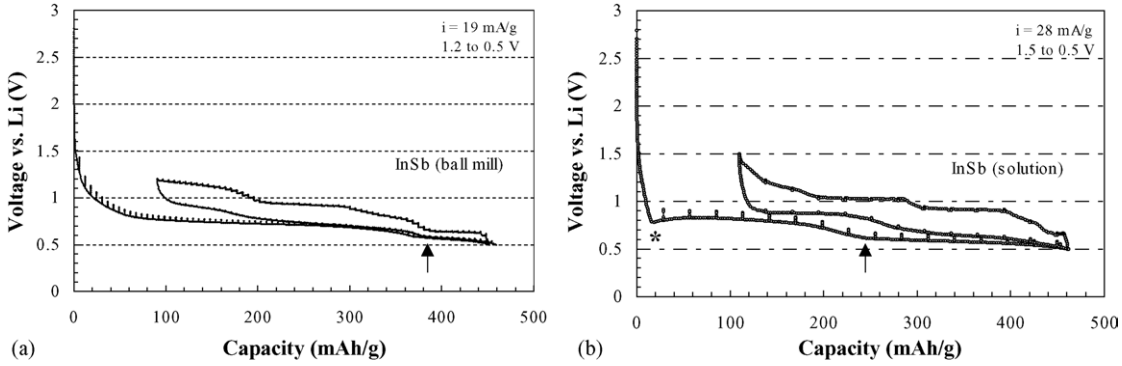

Fig. 9. Voltage profiles (first discharge, and next charge-discharge cycle) of (a) InSb electrode made from ball milling In and Sb and (b) InSb (annealed) produced via the Zn reduction reaction.

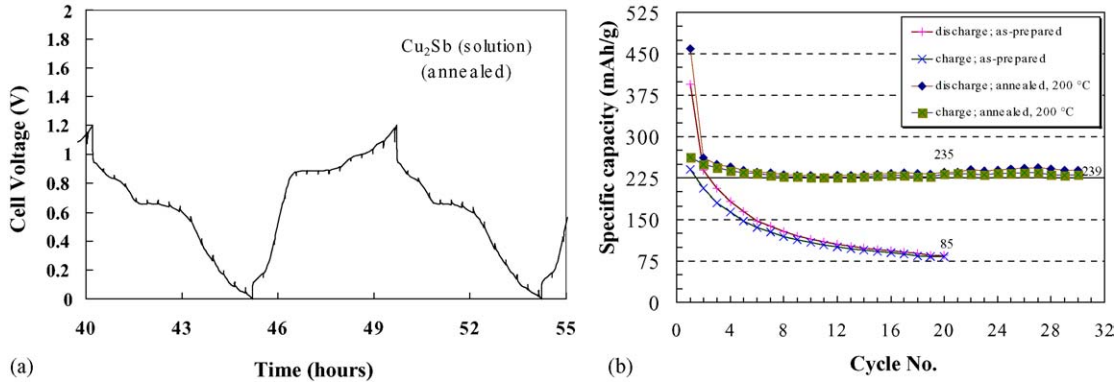

Fig. 11. (a) Voltage profile of Cu_2Sb electrode and (b) capacity plots of the annealed vs. as-precipitated (un-annealed) Cu_2Sb materials.

containing component in these samples (Fig. 8). One hypothesis is that the component of the dendrite, which decomposes under vacuum in the beam, is an amorphous organometallic compound, such as those that might possibly form by reaction of the metal salts with ethylene glycol, e.g., $Cu_3((CH_2CH_2)O_2)_3$ [23,24]. This hypothesis was tested by thermogravimetric analysis to monitor any mass loss of the samples as a result of the evolution of volatile organic species. A significant mass loss between 3 and 9% was observed by heating the InSb, Cu_6Sn_5 and Cu_2Sb samples under argon at 500 °C for 4 h (Table 2). The formation of some In_2O_3 and Sb_2O_3 in the preparation of InSb and Cu_2Sb is perhaps not surprising because it can be expected that nanoparticulate In and Sb deposited by the solution method would be extremely reactive and sensitive to oxidation; the origin of the oxygen that is involved in these reactions is unknown at the present time.

3.4. Electrochemical cycling

The voltage profiles of a lithium cell with an annealed InSb electrode synthesized by the solution route versus a cell containing a ball-milled InSb electrode are compared in Fig. 9a and b. The mechanism of reaction of Li and InSb has already been discussed in detail [4]. In general, the shapes of the curves are similar apart from the profile of the initial discharge to 0.5 V. A long voltage plateau from 0.8 to 0.6 V, corresponding to ~370 mAh g^{-1} of capacity, is observed on the first discharge of the Li/InSb (ball-milled) cell consistent with earlier work (Fig. 9a) [15,25–26]. The next plateau from 0.6 to 0.5 V, which is attributed to the lithiation of extruded In, corresponds to 90 mAh g^{-1}. By contrast, the 0.8–0.6 V plateau of cells containing an InSb electrode made by the solution method, corresponds to only ~225 mAh g^{-1} (Fig. 9b), whereas 215 mAh g^{-1} is delivered between 0.6 and 0.5 V. The higher capacity delivered at the lower voltage can be attributed to the additional indium in the electrode produced by the electrochemical reduction of the In_2O_3 impurity in the sample. The InSb electrode (solution route sample) shows a dip in the voltage profile at ~0.78 V at the onset of the first plateau (indicated by an asterisk in Fig. 9b). This voltage dip is attributed to a diffusion overpotential as a result of nucleation and growth phenomena occurring at the electrode [27]. This nucleation reaction appears to be more prevalent in InSb electrodes comprised of smaller particles made by the solution route method compared to InSb particles synthesized by ball milling. After the first cycle, new plateaus appear above ~0.6 V; they are attributed, at least in part, to ternary phases within the $Li_{3x}In_{1-x}Sb$ electrode (e.g., $x = 0.5$, 0.67) [12,28]; these phases exist along the "line of compensation" [29] in the Li–In–Sb phase diagram and are present in InSb electrodes made either by ball milling or by the solution route.

The capacity of InSb and Cu_6Sn_5 electrodes produced by the solution route is plotted as a function of cycle number in Fig. 10. The electrodes show a first cycle capacity loss of 24 and 22%, respectively. After the first cycle, Cu_6Sn_5 shows superior cycling stability to InSb.

The voltage profile of a typical Li/Cu_2Sb cell containing an annealed Cu_2Sb electrode is shown in Fig. 11a and the capacity versus cycle number plot for the cell in Fig. 11b. These electrodes provided the most stable cycling behavior; the data are comparable to those reported by Fransson et al. for ball-milled Cu_2Sb samples [7]. Annealed Cu_2Sb electrodes (200 °C, under argon) provided greatly improved cycling over un-annealed electrodes yielding 235 mAh g^{-1} after 20 cycles, whereas the un-annealed electrode yielded 85 mAh g^{-1} after the same number of cycles (Fig. 11b). However, both un-annealed and annealed Cu_2Sb electrodes exhibited a large irreversible capacity (40–43%) on the first charge/discharge cycle.

4. Conclusions

Nanoparticulate intermetallic compounds InSb, Cu_6Sn_5 and Cu_2Sb were synthesized at room temperature by an electroless redox process using metal salts dissolved in ethylene glycol with Zn metal as the reducing agent. The nanoparticles have dendritic morphologies, large surface areas and a range of sizes that is dictated by the Zn particle size used. TEM, XRD and thermogravimetric analyses indicate unre-

acted metals, metal oxides and volatile components in the reaction products. Annealing the products under an inert atmosphere increases the yield of the targeted intermetallic phase; it also improves the purity of the samples. The electrochemical performance of the intermetallic electrodes is limited by the first-cycle irreversible capacity loss and the fade rate of the cells; these phenomena are associated with the high surface area of the electrodes and their high reactivity with the electrolyte solution. The Cu_2Sb electrode exhibited the best capacity and cycling stability, delivering a steady 230–240 mAh g^{-1} for 30 cycles between 1.2 and 0 V versus Li^0 after the initial charge/discharge cycle.

Acknowledgments

Financial support from the Office of Basic Energy Sciences and the Office of FreedomCar and Vehicle Technologies of the U.S. Department of Energy under Contract Nos. W31-109-Eng-38 and DE- AC03-76SF00098 subcontract no. 6517749 is gratefully acknowledged. T.S. acknowledges financial support through a grant from the Thai government.

References

[1] K.D. Kepler, J.T. Vaughey, M.M. Thackeray, Electrochem. Solid State Lett. 2 (1999) 307.
[2] L.M.L. Fransson, J.T. Vaughey, K. Edström, M.M. Thackeray, J. Electrochem. Soc. 150 (2003) A86.
[3] I. Rom, M. Wachtler, I. Papst, M. Schmied, J.O. Besenhard, F. Hofer, M. Winter, Solid State Ionics 143 (2001) 329.
[4] H. Tostmann, A.J. Kropf, C.S. Johnson, J.T. Vaughey, M.M. Thackeray, Phys. Rev. B. 66 (2002) 014106.
[5] J.T. Vaughey, L.M.L. Fransson, H.A. Swinger, K. Edstrom, M.M. Thackeray, J. Power Sources 119 (2003) 64.
[6] O. Mao, R.A. Dunlap, J.R. Dahn, J. Electrochem. Soc. 146 (1999) 405.
[7] L.M.L. Fransson, J.T. Vaughey, R. Benedek, K. Edstrom, J.O. Thomas, M.M. Thackeray, Electrochem. Commun. 3 (2001) 317.
[8] R. Alcantara, F.J. Fernandez-Madrigal, P. Lavela, J.L. Tirado, J.C. Jumas, J. Olivier-Fourcade, J. Mater. Chem. 9 (1999) 2517.
[9] R.A. Huggins, in: J.O. Besenhard (Ed.), Handbook of Battery Materials, Wiley-VCH, Wienheim, Germany, 1999, Part III.1, p. 359.
[10] I. Kim, P.N. Kumta, G.E. Blomgren, Electrochem. Solid State Lett. 3 (2000) 493.
[11] J. Wolfenstine, S. Campos, D. Foster, J. Read, W.K. Behl, J. Power Sources 109 (2002) 230.
[12] T. Sarakonsri, Ph.D. Thesis, Michigan Technological University, 2002.
[13] A. Trifonova, M. Wachtler, M.R. Wagner, H. Schroettner, Ch. Mitterbauer, F. Hofer, K.-C. Möller, M. Winter, J.O. Besenhard, Solid State Ionics 168 (2004) 51.
[14] H. Li, G. Zhu, X. Huang, L. Chen, J. Mater. Chem. 10 (2000) 693.
[15] J.T. Vaughey, J. O'Hara, M.M. Thackeray, Electrochem. Solid State Lett. 3 (2000) 13–16.
[16] JCPDS Database: InSb, JCPDS reference card #06-0208, In_2O_3 JCPDS reference card #44-1087, In JCPDS reference card #05-0642, Cu_6Sn_5 JCPDS reference card #02-0713, Cu_3Sn JCPDS reference card #01-1240, Sn JCPDS reference card #19-1365, Cu_2Sb JCPDS reference card #03-1023, Sb JCPDS reference card #35-0782, Sb_2O_4 JCPDS reference card #75-1566.
[17] Y. Shao-Horn, S.A. Hackney, B.C. Cornilsen, J. Electrochem. Soc. 144 (1997) 3147.
[18] L. Fransson, E. Nordstrom, K. Edström, L. Haggstrom, J.T. Vaughey, M.M. Thackeray, J. Electrochem. Soc. 149 (2002) A736.
[19] H. Li, L. Shi, Q. Wang, L. Chen, X. Huang, Solid State Ionics 148 (2002) 247.
[20] B.D. Cahan, D. Scherson, M.A. Reid, J. Electrochem. Soc. 135 (1988) 285.
[21] C.S. Johnson, M.M. Thackeray, unpublished data.
[22] (a) P.H. Leo, W.W. Mullins, R.F. Sekerka, J. Vinals, Acta Metall. et Mater. 38 (1990) 1573;
(b) J.M. Rickman, J. Vinals, R.F. Sekerka, W.W. Mullins, Phys. Rev. B 45 (1992) 7750.
[23] F. Fievet, F. Fievet-Vincent, J.P. Lagier, B. Dumont, M. Figlarz, J. Mater. Chem. 3 (1993) 627.
[24] Dictionary of Organometallic Compounds, vol. II, Chapman & Hall, 1984.
[25] C.S. Johnson, J.T. Vaughey, M.M. Thackeray, T. Sarakonsri, S.A. Hackney, L. Fransson, K. Edstrom, J.O. Thomas, Electrochem. Commun. 2 (2000) 595.
[26] D. Larcher, L.Y. Beaulieu, D.D. MacNeil, J.R. Dahn, J. Electrochem. Soc. 147 (2000) 1658.
[27] R.A. Huggins, J. Power Sources 81–82 (1991) 13.
[28] W. Sitte, W. Weppner, Z. Naturforsch 42 (1987) 1.
[29] A.J. Kropf, H. Tostmann, C.S. Johnson, J.T. Vaughey, M.M. Thackeray, Electrochem. Commun. 3 (2001) 244.